Phys Chem Minerals (2002) 29: 609–616
DOI 10.1007/s00269-002-0273-3


ORIGINAL PAPER

M. Zhang · G. J. Redhammer · E. K. H. Salje
M. Mookherjee

# $LiFeSi_2O_6$ and $NaFeSi_2O_6$ at low temperatures: an infrared spectroscopic study

Received: 21 January 2002 / Accepted: 22 July 2002

**Abstract** Synthetic aegirine $LiFeSi_2O_6$ and $NaFeSi_2O_6$ were characterized using infrared spectroscopy in the frequency range 50–2000 $cm^{-1}$, and at temperatures between 20 and 300 K. For the $C2/c$ phase of $LiFeSi_2O_6$, 25 of the 27 predicted infrared bands and 26 of 30 predicted Raman bands are recorded at room temperature. $NaFeSi_2O_6$ (with symmetry $C2/c$) shows 25 infrared and 26 Raman bands. On cooling, the $C2/c$–$P2_1/c$ structural phase transition of $LiFeSi_2O_6$ is characterized by the appearance of 13 additional recorded peaks. This observation indicates the enlargement of the unit cell at the transition point. The appearance of an extra band near 688 $cm^{-1}$ in the monoclinic $P2_1/c$ phase, which is due to the Si–O–Si vibration in the $Si_2O_6$ chains, indicates that there are two non-equivalent Si sites with different Si–O bond lengths. Most significant spectral changes appear in the far-infrared region, where Li–O and Fe–O vibrations are mainly located. Infrared bands between 300 and 330 $cm^{-1}$ show unusually dramatic changes at temperatures far below the transition. Compared with the infrared data of $NaFeSi_2O_6$ measured at low temperatures, the change in $LiFeSi_2O_6$ is interpreted as the consequence of mode crossing in the frequency region. A generalized Landau theory was used to analyze the order parameter of the $C2/c$–$P2_1/c$ phase transition, and the results suggest that the transition is close to tricritical.

**Keywords** $LiFeSi_2O_6$ · $NaFeSi_2O_6$ · Infrared spectroscopy · Low temperature · Phase transition

M. Zhang (✉) · E. K. H. Salje · M. Mookherjee
Department of Earth Sciences,
University of Cambridge,
Downing Street, Cambridge, CB2 3EQ, UK
E-mail: mz10001@esc.cam.ac.uk
Tel.: +44-1223-333411
Fax: +44-1223-333450

G. J. Redhammer
Institut für Kristallographie,
Rheinisch Westfälische Technische Hochschule Aachen,
Jägerstraße 17/19, 54056 Aachen, Germany

## Introduction

Li-aegirine ($LiFeSi_2O_6$) is a chain silicate, very similar to the minerals $NaFeSi_2O_6$ (acimite/aegirine) and Li-$AlSi_2O_6$ (spodumene), which have monoclinic symmetry (space group $C2/c$) at room temperature. The structural details were determined by Clark et al. (1969), Behruzi et al. (1984) and Redhammer et al. (2001). The pyroxene structure consists of alternating chains of $SiO_4$ tetrahedra, and ribbons of sixfold-coordinated octahedral bands, parallel to the $c$ axis. Li and Fe occur at two non-equivalent oxygen octahedra, conventionally denoted as M1 and M2. Each ribbon includes a zigzag chain of M1 sites sandwiched between two linear bands of M2 sites.

Low-temperature studies of $LiFeSi_2O_6$ revealed a structural phase transition from $C2/c$ at room temperature condition to $P2_1/c$ at around 228 K (Behruzi et al. 1984). Detailed low-temperature behaviour of the crystal and the magnetic structure has been reported by Redhammer et al. (2001). The low-temperature phase transition for Li-aegirine is accompanied by strong discontinuities in the thermal evolution of the lattice parameters, appearance of the Bragg reflections with $h + k \neq 2n$, distinction of two non-equivalent tetrahedral sites, changes in the Li coordination from 6 at room temperature to 5 at temperatures lower than $T_c$, and a discontinuity in the quadrupole splitting (Redhammer et al. 2001).

We undertook this spectroscopic study to investigate the behaviour of vibrational phonons of $LiFeSi_2O_6$ at low temperatures, and to obtain further understanding of the structural phase transition ($C2/c$ to $P2_1/c$). We found that, upon cooling the structural phase transition is characterized by significant modifications of the infrared spectrum of $LiFeSi_2O_6$, involving the appearance of additional phonon bands and complex frequency changes. To our knowledge, this work is the first systematic low-temperature infrared study on the phase transition of $LiFeSi_2O_6$.

## Experimental

The sample of $LiFeSi_2O_6$ was prepared by solid-state ceramic sintering techniques at 1223 K and ambient pressure. The starting material was a stoichiometric mixture of finely ground $Li_2CO_3$, $Fe_2O_3$ and $SiO_2$. Well-crystallized $LiFeSi_2O_6$ was obtained after several cycles of firing, regrinding and rerunning the sintered material at the given temperature in open platinum crucibles. The synthesis product is yellowish green. The sample was previously characterized by neutron powder diffraction and Mössbauer measurements (Redhammer et al. 2001). The results show that it is monoclinic, with space group $C2/c$, $a = 9.6641(2)$ Å, $b = 8.6612(3)$ Å, $c = 5.2924(2)$ Å, $\beta = 110.12(1)°$ at 300 K.

The sample of $NaFeSi_2O_6$ was prepared through solid-state reaction by ceramic sintering at 1223 K. The starting material for all synthesis was a stoichiometric mixture of $Na_2CO_3$, $Fe_2O_3$ and $SiO_2$ with a slight excess of $SiO_2$. The sample also was previously characterized by Mössbauer spectroscopy and powder X-ray diffraction (Redhammer et al. 2000). The results show that it contains exclusively ferric iron, and is monoclinic with space group $C2/c$, $a = 9.6543(7)$ Å, $b = 8.8070(6)$ Å, $c = 5.2943(4)$ Å and $\beta = 107.316(5)°$ at 300 K. Two additional samples, grown by hydrothermal reaction (Redhammer et al. 2000), were also investigated and show similar Raman spectra, but with relatively weak signals.

Infrared powder pellet technique reported by Zhang et al. (1996) was employed in this study. Polyethylene and CsI were used as matrix materials for the far-infrared measurements, whereas KBr was used for the measurements in the mid-infrared region. Sample/matrix ratios were 1:50, 1:300 and 1:400 for polyethylene, CsI and KBr, respectively. Sample powders were thoroughly mixed with the matrix materials. In order to reduce static charges caused by the mixing, a few drops of pentane were used for the mixing of the sample with polyethylene powder. A certain amount of the mixtures (100, 200 and 300 mg for polyethylene, KBr and CsI, respectively) were pressed into 13-mm discs under vacuum. The sample pellets were used within 12 h of preparation.

Using a Bruker IFS 113v spectrometer, the absorption spectra between 20 and 300 K were recorded under vacuum to avoid absorption from water and carbon oxides in the air. The spectra were measured in three separated regions: (1) 50–400 $cm^{-1}$ (with polyethylene pellets, a DTGS detector, 6- and 25-μm Mylar beamsplitters, a Mercury lamp, a pair of polyethylene windows for a cryostat); (2) 250–700 $cm^{-1}$ (with CsI pellets, a DTGS detector, 3.5-μm Mylar beam-splitter, a Globar lamp, a pair of KRS5 windows for the cryostat) and (3) 500–2000 $cm^{-1}$ (with KBr pellets, a MCT detector, KBr beam-splitter, a Globar lamp, a pair of KRS5 windows for the cryostat). In each spectral range two runs of measurements were performed on cooling, and the spectra were reproducible. Instrumental resolution of 2 $cm^{-1}$ was used in all measurements, and 150 or 200 scans were averaged. A closed-cycle liquid-helium cryostat (LEYBOLD), equipped with KRS5 and polyethylene windows, was used for low-temperature experiments. Two thermal sensors, well calibrated by their manufacturers, were used in the cryostat. One was used to control the cryostat and the other for measuring the sample temperature. The temperature stability was better than 1 K.

FT-Raman spectra of $LiFeSi_2O_6$ and $NaFeSi_2O_6$ were recorded in the region of 50–2000 $cm^{-1}$ at room temperature using a Bruker IFS 66v spectrometer equipped with a Bruker FRA 106 FT-Raman accessory. A silicon-coated calcium fluoride beam-splitter and radiation of 1064 nm from a Nd:YAG laser were used. A liquid nitrogen-cooled, high-sensitivity Ge detector was used. The spectrum was recorded with a laser power of 120 mW and a backscattering geometry. An instrumental resolution of 2 $cm^{-1}$ and 1024 scans was adopted. Software OPUS-IR (Bruker) was used for data analysis and curve fittings.

## Results and discussion

The room-temperature infrared and Raman spectra of $LiFeSi_2O_6$ are shown in Fig. 1. In the $C2/c$ ($C_{2h}^6$) phase of $LiFeSi_2O_6$, there are 20 atoms in the primitive unit cell; 57 optical vibrational modes are expected (Rutstein and White 1971; Wang et al. 2001): $14A_g + 16B_g + 13A_u + 14B_u$. The $A_g$ and $B_g$ modes are Raman-active, whereas the $A_u$ and $B_u$ modes are infrared-active. Therefore, there are 27 modes infrared-active and 30 Raman-active. In this study, 25 infrared bands were detected, whereas 26 Raman bands were resolved (the peak near 84 $cm^{-1}$ in the Raman spectrum is an artefact from the instrument). The peak positions of the infrared and Raman bands observed are listed in Table 1. The vibrational bands of $LiFeSi_2O_6$ can be grouped into different frequency regions with characteristic vibrations, although assigning all the individual vibrational modes of $LiFeSi_2O_6$, especially in far-infrared region, appears difficult or even impossible at this stage. Based

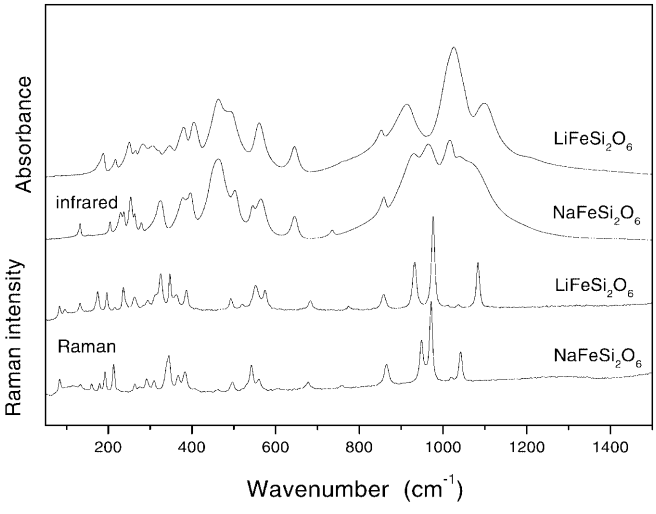


**Fig. 1** Room-temperature infrared and Raman spectra of $LiFeSi_2O_6$ and $NaFeSi_2O_6$ between 50 and 1400 $cm^{-1}$. The infrared spectrum was merged using the data measured in different frequency ranges. The peak positions of the spectra are listed in Table 1

**Table 1** Observed Raman and infrared band positions (in units of $cm^{-1}$) of Li-aegirine ($LiFeSi_2O_6$). The peak positions were determined by the secondary-derivative method

| | | | | | | | | | | | | | |
|---|---|---|---|---|---|---|---|---|---|---|---|---|---|
| Raman (293 K) | 97 | 133 | 175 | 196 | 214 | 237 | 263 | 284 | 294 | 313 | 325 | 347 | 363 |
| | 387 | 493 | 519 | 553 | 575 | 684 | 776 | 857 | 932 | 976 | 1012 | 1038 | 1084 |
| Infrared (293 K) | 175 | 188 | 217 | 246 | 251 | 265 | 285 | 307 | 323 | 345 | 380 | 401 | 409 |
| | 461 | 497 | 561 | 645 | 759 | 774 | 785 | 854 | 916 | 1016 | 1026 | 1096 | |
| Infrared (20 K) | 167 | 183 | 193 | 215 | 224 | 231 | 251 | 259 | 267 | 287 | 295 | 302 | 321 |
| | 326 | 329 | 352 | 380 | 397 | 411 | 452 | 463 | 491 | 513 | 538 | 562 | 651 |
| | 688 | 762 | 769 | 779 | 788 | 848 | 914 | 985 | 1009 | 1021 | 1066 | 1092 | 1138 |

on previous infrared and Raman work on silicates and $Si_2O_6$ chain units, and theoretical modelling (Saksena 1961; Saksena et al. 1963; Lazarev 1972; Farmer 1974; McMillan 1984), we classify the observed bands into four frequency regions. (1) The bands between 800 and 1200 $cm^{-1}$ are assigned as the Si–O stretching vibrations related to the non-bridged Si–O bonds in the $SiO_4$ tetrahedra. (2) The bands between 650 and 800 $cm^{-1}$ are mainly attributed to the vibrations related to the bridged Si–O–Si vibrations within the $Si_2O_6$ chains. Vibrational spectra from silicates have shown that bands in this region are sensitive to Si–O–Si linkages (McMillan 1984; Mysen 1990). Raman data of monoclinic/orthorhombic pyroxene and triclinic pyroxenoid (Huang et al. 2000; Wang et al. 2001) showed characteristic bands in this frequency region, and these authors assigned the bands as the contributions of the chain units. (3) The Si–O bending bands of $SiO_4$ tetrahedra are mainly located between 425 and ~650 $cm^{-1}$. The assignment of an IR band near 645 $cm^{-1}$ (with the highest frequency in this region) is not straightforward and further work might be needed to clarify this issue. We attribute it to Si–O bending rather than vibration related to $Si_2O_6$ chains, because only three IR bands are expected to be associated with the relative motions of $SiO_4$ within the $[Si_2O_6]_n$ chains in the $C2/c$ phase (Wang et al. 2001) and this band shows an intensity very different to the bands near 759, 774 and 785 $cm^{-1}$. Furthermore, the substitution of Li by Na does not result in a significant change of its band frequency (Table 1) while the differences of the O3–O3–O3 bridge angle and the Si–O3 bond lengths between $LiFeSi_2O_6$ (Redhammer et al. 2001) and $NaFeSi_2O_6$ (Redhammer and Roth 2002) are significant.

(4) The bands between 50 and 425 $cm^{-1}$ are of complex nature, mainly due to lattice vibration bands that are related to Li–O and Fe–O interactions as well as possible Si–O bending. In a Raman study on Mg–Fe–Ca pyroxenes (e.g. enstatite, fesilite, diopside, hedenbergite and wollastonite), Huang et al. 2000 reported M–O (M cations) stretching vibrations between 200 and 450 $cm^{-1}$. An investigation of the density state of $Mg_2Si_2O_6$ shows that cations mainly attribute vibrations in the far-infrared region (Choudhury et al. 1998). Synthesis and analysis of Li isotope samples are desirable and would be helpful for gaining better understanding of the individual far-infrared bands in $LiFeSi_2O_6$.

The effect of cooling on the infrared spectrum of $LiFeSi_2O_6$ is characterized by band-sharpening, shift in frequency and increase in intensity (Fig. 2a–c). The transition from $C2/c$ to $P2_1/c$ involves the enlargement of the primitive unit cell. In its $P2_1/c$ phase, $LiFeSi_2O_6$ has double the number of chain units of $[Si_2O_6]_n$ per primitive unit cell and therefore double the number of atoms that contribute to vibrational modes; 57 modes are expected infrared-active whereas 60 Raman-active ($30A_g + 30B_g + 29A_u + 28B_u$). The structural phase transition ($C2/c \rightarrow P2_1/c$) near 230 K is evidenced by the appearance of extra bands at 154, 213, 232, 280, 302, 453, 508, 537, 688, 768, 985, 1068 and 1138 $cm^{-1}$ (Fig. 2a–c). Two more bands near 326 and 329 $cm^{-1}$ are recorded below 60 K. A total of 39 infrared bands are found at 20 K. Some predicted infrared bands may be too weak or too overlaid to be resolved even at low temperatures.

Peak positions of infrared data at low temperatures were obtained using the second-derivative or curve-fitting methods. For the case of curve-fitting, the measured data were fitted to the Lorentzian function with linear baselines. The positions as a function of temperature are shown in Fig. 3a–c. The low-frequency lattice bands show a very significant frequency shift upon cooling. For example, the lowest-frequency band exhibits an increase of frequency from 154 $cm^{-1}$ at 220 K to 167 $cm^{-1}$ at 20 K (with a relative frequency increase of 8.4%).

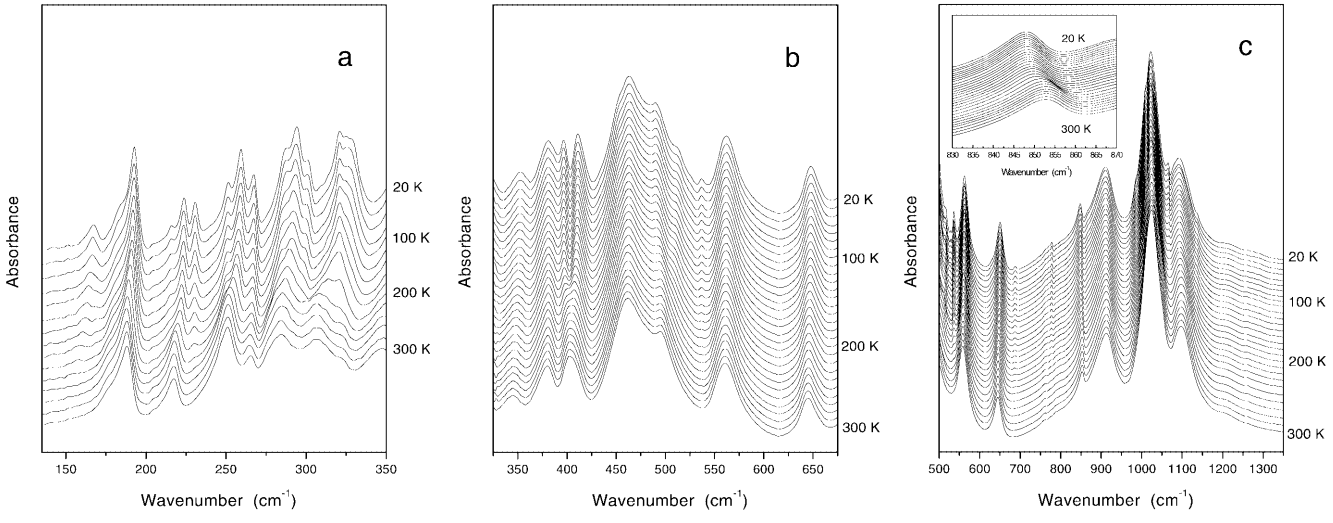


**Fig. 2a–c** Temperature evolution of infrared spectra between 20 and 300 K. **a** In the region of 135–335 $cm^{-1}$ (with polyethylene pellets; no infrared bands of $LiFeSi_2O_6$ were recorded between 50 and 135 $cm^{-1}$; temperature interval = 20 K); **b** In the region of 325–675 $cm^{-1}$ (with CsI pellets, temperature interval = 10 K); **c** Between 500 and 1350 $cm^{-1}$ (with KBr pellets, temperature interval = 10 K). The *inset* shows the detailed changes for the Si–O stretching band near 852 $cm^{-1}$ between 20 and 300 K. The temperature interval is 10 K

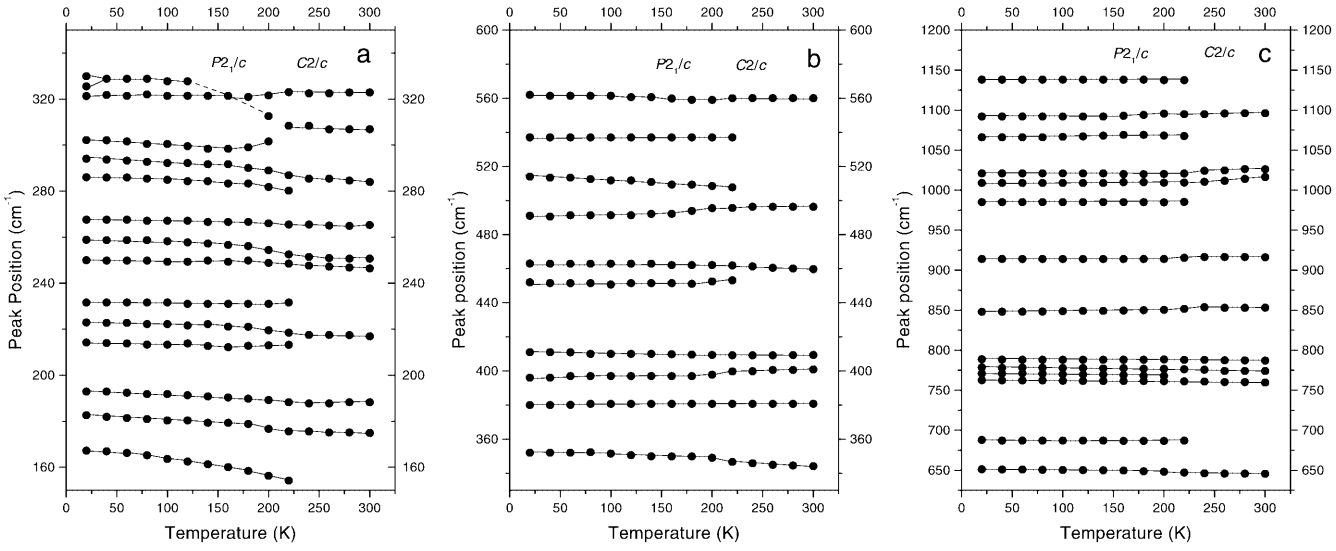


**Fig. 3a–c** Peak positions as a function of temperature between 20 and 300 K. **a** Between 150 and 350 $cm^{-1}$. **b** Between 330 and 600 $cm^{-1}$. **c** Between 625 and 1200 $cm^{-1}$. The *lines* are visual guides, and the *dashed lines* are used between 300 and 330 $cm^{-1}$ to reflect the difficulty in tracing the change of the individual bands in the region

With decreasing temperature from 220 to 20 K, the 175 $cm^{-1}$ band shifts to 183 $cm^{-1}$ and the 188 $cm^{-1}$ band increases its frequency to 193 $cm^{-1}$ (with relative changes of 4.6 and 2.7%, respectively). However, the frequencies of the Si–O stretching bands of $SiO_4$ tetrahedra show little temperature dependence on cooling. When the sample is cooled from 220 K to 20 K, the Si–O bands near 1096, 1068 and 851 $cm^{-1}$ show frequency changes of −0.27, −0.18, and −0.35%, respectively (the negative values indicate decrease in frequency on cooling), whereas the Si–O bands near 1009, 985 and 916 $cm^{-1}$ exhibit no detectable frequency shifts. This suggests that the $SiO_4$ tetrahedra are essentially rigid and that the bond distances between Si and O do not significantly change on cooling. The observation is consistent with structural refinements from X-ray measurements (Redhammer et al. 2001), which showed an almost unchanged average Si–O distance of ~1.622 Å at low temperatures. One of the interesting observations in this study is the IR band near 688 $cm^{-1}$ in the $P2_1/c$ phase of $LiFeSi_2O_6$. Wang et al. (20001) compared with Raman data of different types of pyroxenes and pyoxeniods ($C2/c$ monoclinic, $P2_1/c$ monoclinic, $P\bar{1}$ triclinic and *Pbca* orthorhombic), and reported that the Raman bands near ~670 $cm^{-1}$ are associated with chain structures. These authors found that pyroxenes with a single-chain structure (e.g. $C2/c$ monoclinic and $P\bar{1}$ triclinic) generally have only one peak near ~670 $cm^{-1}$, while pyroxenes with two chains (e.g. $P2_1/c$ monoclinic and *Pbca* orthorhombic) commonly show a doublet near ~670 $cm^{-1}$. This finding was used to distinguish different types of pyroxenes. Based on their observations, we consider that the appearance of the IR band near 688 $cm^{-1}$ in the $P2_1/c$ phase of $LiNaSi_2O_6$ is associated with new Si–O–Si vibrations of the $Si_2O_6$ chains, and this signal indicates the formation of two independent silicate chains as observed by Behruzi et al. (1984) and Redhammer et al. (2001). A similar observation of an additional Si–O–Si signal in the region of 600–750 $cm^{-1}$ was also reported in a high-pressure Raman study of the $C2/c$–$P2_1/c$ phase transition in (Mg, Fe)$SiO_3$ clinopyroxenes (Ross and Reynard 1999).

One of the important and complex spectral variations is the change associated with the bands between 300 and 330 $cm^{-1}$ with decreasing temperature. These bands show significant modifications in peak profiles near the transition temperature in response to the structure change. However, it is strange that only one local maximum is revealed at 160 K (Fig. 2a), although several bands are revealed in the region at higher or lower temperatures. The signal exhibits further dramatic variations at temperatures far below the transition temperature. As shown in Fig. 2a, a shoulder near 327 $cm^{-1}$ starts to develop below 120 K or becomes more active (Figs. 2a and 3a. The dashed lines in Fig. 3a represent only uncertain visual links between the data points), while other phonon bands do not appear to show further change on cooling. The feature unexpectedly becomes two local maxima near 325 and 328 $cm^{-1}$ at 20 K. This different temperature dependence between the bands in 300–350 $cm^{-1}$ and those in the other frequency regions cannot be simply explained by temperature-induced sharpening and band shift. We initially suspected that the change was associated with Li motion, as Li–O bands can be located between 250 and 400 $cm^{-1}$ and temperature-induced positional order/disorder caused by Li motion/hopping has commonly been reported in Li materials (Teeters and Frech 1982; Zhang et al. 1998; Zhigadlo et al. 2001). As a result of the order/disorder, the dielectric constants, IR and Raman spectra could show significant variation.

In order to gain better understanding of the nature of these $LiFeSi_2O_6$ bands between 300 and 350 $cm^{-1}$ (Fig. 2a), we measured $NaFeSi_2O_6$, a clinopyroxene with

crystal structure similar to $LiFeSi_2O_6$. At room temperature, $NaFeSi_2O_6$ is also monoclinic ($C2/c$ interchain Fe–Fe distance = 3.188 and 5.435 Å, bridge angle Fe–O–Fe = 100.7°, tetrahedra chain angle O3–O3–O3 = 174.19°) (Clark et al. 1969; Redhammer et al. 2000). The substitution of Li by Na changes the coordination number of the M2 site from 6 to 8, resulting in a structural expansion and an increase in interchain distances. The room-temperature infrared and Raman spectra of $NaFeSi_2O_6$ are shown in Fig. 1. For $NaFeSi_2O_6$, 25 infrared bands and 26 Raman bands are recorded at room temperature. The infrared spectrum from this study is consistent with reported data between 450 and 1200 $cm^{-1}$ on $NaFeSi_2O_6$ (Lazarev 1972), although our data extend to the far-infrared region. The peak positions are listed in Table 2. In the far-infrared region where the bands are mainly attributed to lattice vibrations, both infrared and Raman spectra of $NaFeSi_2O_6$ exhibit features different from those of $LiFeSi_2O_6$, because of the change of the coordination number of the M2 site and local structural modifications. The substitution of Li by Na shows relatively weak influence on the Si–O bands. The differences between the two materials are better revealed in Raman spectra because of their relatively sharp and well-resolved bands. Between 400 and 1100 $cm^{-1}$, the essential Raman pattern of $LiFeSi_2O_6$ is still preserved in $NaFeSi_2O_6$ although the substitution leads to a frequency shift. The Si–O deformation or bending near 493 $cm^{-1}$ shifts to 497 $cm^{-1}$. The Raman bands related to the Si–O–Si vibrations in the $Si_2O_6$ chains give values of 684 and 776 $cm^{-1}$ for $LiFeSi_2O_6$ and 678 and 760 $cm^{-1}$ in $NaFeSi_2O_6$. This is associated not only with the different O3–O3–O3 angles in the two materials (180.83° for $LiFeSi_2O_6$ and 174.0° for $NaFeSi_2O_6$), but also the Si–O3 interactions. The Si–O stretching bands of $SiO_4$ tetrahedra between 850 and 1100 $cm^{-1}$ show different frequency changes. The two intense Si–O stretching Raman bands with highest frequencies (1084 and 976 $cm^{-1}$) in $LiFeSi_2O_6$ show lower frequency values (1043 and 971 $cm^{-1}$) in $NaFeSi_2O_6$ (Tables 1 and 2), whereas the Si–O stretching bands near 932 and 857 $cm^{-1}$ show an increase in frequency to 948 and 865 $cm^{-1}$. This observation indicates a complex impact of the substitution on the framework of the clinopyroxene group and complicated interactions between Si, O and cations.

The effect of cooling on the far-infrared spectrum of $NaFeSi_2O_6$ is weak compared to that in $LiFeSi_2O_6$ (Fig. 4). Between 20 and 300 K, we observed no spectral changes in $NaFeSi_2O_6$, which may suggest the $C2/c$ to $P2_1/c$ transition as revealed in $LiFeSi_2O_6$. Our observation is consistent with the result of Redhammer and Roth (2002). Analyzing the band near 254 $cm^{-1}$, which shows the strongest frequency change (it shifts to 257 $cm^{-1}$ at 20 K) in the far-infrared region, reveals a continuous frequency change as a function of temperature. We noted, like $LiFeSi_2O_6$, local maxima near 326 and 328 $cm^{-1}$ occurred above 40 K in $NaFeSi_2O_6$ (Fig. 4). This observation could suggest that the appearance of the 322 and 325 bands in $LiFeSi_2O_6$ is probably not due to potential Li ordering at low temperatures as seen in other Li materials. Although at 20 K $LiFeSi_2O_6$ and $NaFeSi_2O_6$ have different structural symmetries, the occurrence of the similar spectral features between 310 and 340 $cm^{-1}$ in both materials appears to imply that the anomaly in $LiFeSi_2O_6$ near 20 K is probably related to the behaviour of Fe. Antiferromagnetic ordering in both $LiFeSi_2O_6$ and $NaFeSi_2O_6$ was observed at low temperatures (near 20 K) and it was characterized by change of temperature dependence of magnetic susceptibility and the appearance of a magnetic ordered six-line spectrum due to magnetic hyperfine interactions (Baum et al. 1988; Lottermoser et al. 1998; Redhammer et al. 2001). These authors also observed distinct preordering phenomena up to 35 K and reported that at the magnetic phase transition the unit-cell parameters exhibited a pronounced magneto-striction of the lattice. The ordering might be responsible for the spectra change near 20 K. However, the systematic spectral change in the region of 310–340 $cm^{-1}$ at temperatures between 60 and 200 K can hardly be explained by the antiferromagnetic ordering because the temperature region is too high (the antiferromagnetic ordering

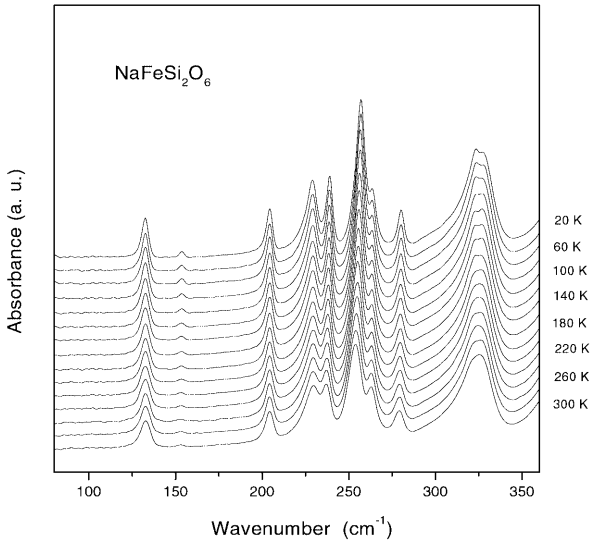


**Fig. 4** Temperature dependence of infrared spectra of $NaFeSi_2O_6$ in the frequency region of 80 and 360 $cm^{-1}$ between 20 and 300 K (with polyethylene pellets, temperature interval of 20 K)

**Table 2** Observed Raman and infrared band positions (in units of $cm^{-1}$) of $NaFeSi_2O_6$

| | | | | | | | | | | | | | |
|---|---|---|---|---|---|---|---|---|---|---|---|---|---|
| Raman | 116 | 133 | 160 | 178 | 192 | 242 | 263 | 275 | 292 | 310 | 339 | 345 | 367 |
| (293 K) | 383 | 406 | 460 | 497 | 542 | 561 | 678 | 760 | 865 | 948 | 971 | 1021 | 1043 |
| Infrared | 133 | 153 | 204 | 229 | 237 | 254 | 263 | 279 | 322 | 328 | 378 | 388 | 397 |
| (293 K) | 463 | 503 | 545 | 564 | 646 | 736 | 859 | 929 | 966 | 1018 | 1040 | 1069 | |

in $NaFeSi_2O_6$ does not cause significant spectral changes between 60 and 200 K). Structural studies on $LiFeSi_2O_6$ (e.g. Redhammer et al. 2001) showed that Fe–O exhibited very weak changes on cooling, therefore the antiferromagnetic ordering is unlikely to cause the dramatic spectral variations between 60 and 200 K (Fig. 2a). We consider that the far-infrared spectral change between 60 and 200 K in $LiFeSi_2O_6$ is related to a complex mode crossing. As shown by the dashed lines in Fig. 3a, these phonon frequencies appear to cross one another on cooling. Similar crossing behaviour has been reported in other materials (Cho and Jang 2000). As a result of the crossing, the related spectral feature, as well as phonon frequencies and widths could be significantly modified.

In order to gain a better understanding of the phase transition, the order parameter, $Q$, related to the structural phase transition from $C2/c$ to $P2_1/c$ in $LiFeSi_2O_6$, was extracted from the infrared data. According to hard mode spectroscopy, changes of frequency, width and intensity (i.e. $\Delta\omega$, $\Delta$Ggr; and $\Delta A$) may be proportional to $Q^2$ and $Q^4$ (Salje and Bismayer 1997). Results from X-ray diffraction measurement (Redhammer et al. 2001) were used to clarify the case. The comparison of the changes in the cell volume (the volume change is related to $Q^2$) and the Si–O stretching band near 825 $cm^{-1}$ on cooling (the detailed temperature evolution of the 825 $cm^{-1}$ band can be seen in the inset of Fig. 2c) is shown in Fig. 5, where the reduced data are used for a better comparison. The data from infrared and X-ray diffraction measurements in Fig. 5 show essentially similar behaviours at low temperatures. Thus, it is reasonable to consider that for $LiFeSi_2O_6$ the change in phonon profiles is related to $Q^2$. The integrated absorbance of the infrared bands at 538 and 688 $cm^{-1}$ was used to work out the order parameter. These bands were chosen, because they are absent in the $C2/c$ phase (no need to perform an extrapolation of the $C2/c$ data and to predict their changes in the lower temperature region) and it is easy to determine the zero value of $Q$ (unlike their frequencies and widths, the integrated absorbance of these bands becomes zero when approaching the transition). The temperature dependence of the order parameter (plotted as $Q^4$) is shown in Fig. 6 (the inset in Fig. 6 indicates the temperature evolution of the 688 $cm^{-1}$ band). The behaviour of the order parameter as a function of temperature can be described by the Landau theory. It is well understood that near phase transitions, the Landau free energy can be written as Eq. (1) (Landau and Lifshitz 1980). As the quadratic term may be negative, the sixth-order term in the free energy expansion is needed so that the series expansion of $G(Q)$ converges, giving (for first-order transitions):

$$\Delta G(Q) = \frac{1}{2}A(T_c - T)Q^2 + \frac{1}{4}BQ^4 + \frac{1}{6}CQ^6 \ , \qquad (1)$$

where $A$, $B$ and $C$ are coefficients, and $T_c$ and $Q$ are the transition temperature and the order parameter, respectively. When $B$ or $C = 0$, the Eq. (1) can be used for tricritical or second-order phase transitions.

For different types of phase transitions, the order parameter, $Q$, can be expressed as

$$Q^2 = \left[\frac{A}{C}(T_c - T)\right]^{2\beta}, \ \beta = 0.25 \quad \text{(tricritical)} \qquad (2)$$

$$Q^2 = \left[\frac{A}{B}(T_c - T)\right]^{2\beta}, \ \beta = 0.5 \quad \text{(second-order)} \qquad (3)$$

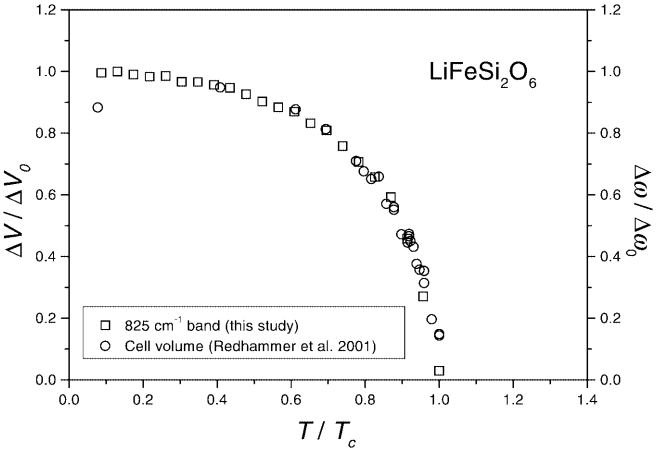


**Fig. 5** Comparison of reduced changes of Si–O stretching band at 825 $cm^{-1}$ ($\Delta\omega/\Delta\omega_0$) and change of cell volume ($\Delta V/\Delta V_0$) at low temperatures. The cell volume data are from Redhammer et al. (2001). The difference in cell volume or frequency was obtained by fitting the data at temperatures above the transition to quadratic functions and extrapolating their value to the region below the transition. $\Delta\omega_0$ and $\Delta V_0$ correspond to the values extrapolated to 0 K ignoring the possible influence of the antiferromagnetic ordering below 20 K

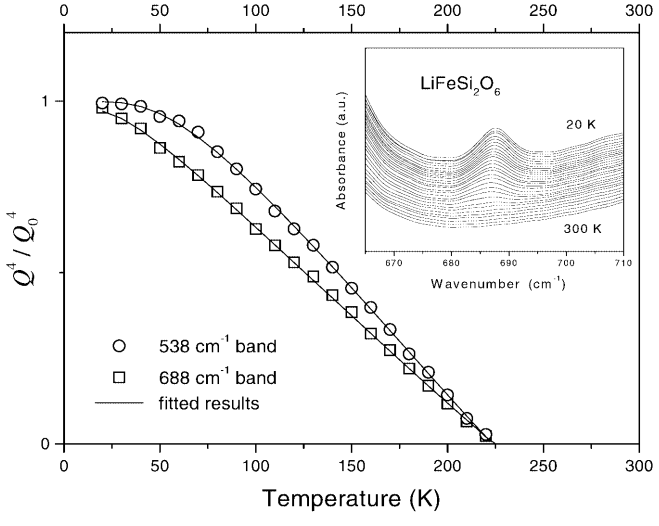


**Fig. 6** Temperature dependence of the order parameter $Q$, which was obtained from the integrated absorbance of the bands near 538 and 688 $cm^{-1}$ (frequency value for 20 K) in $LiFeSi_2O_6$. The *open symbols* represent the data from our infrared measurements. The *solid lines* are the results from fitting the measured data to a generalized Landau theory (see text for details). The fitting gives $\beta = 0.26 \pm 0.02$, and $T_c = 226 \pm 3$ K. The *inset* shows the temperature evolution of the 688 $cm^{-1}$ band at temperatures between 20 and 300 K. The temperature interval is 10 K

$$Q^2 = \frac{1}{2}C\{-B + [B^2 - 4AC(T_c - T)]^{\frac{1}{2}}\} \quad . \quad \text{(first-order)} \tag{4}$$

Since the Landau free energy is an expansion of the free energy for small values of $Q$, the traditional Landau theory may not well describe the behaviour of the order parameter in the region far from the transition. Furthermore, the order parameter may become saturated at very low temperatures because the third law of thermodynamics requires that the order parameter become independent to temperature near absolute zero temperature. Salje et al. (1991a,b) proposed a generalized Landau theory for large $Q$ and it demonstrated a good description of phase transitions for second order and in the form of

$$\Delta G = \frac{1}{2}A\theta_s[\coth(\frac{\theta_s}{T_c}) - \cot\mathrm{h}(\frac{\theta_s}{T})]Q^2 + \frac{1}{4}BQ^4 + \frac{1}{6}CQ^6 \quad . \tag{5}$$

In this generalized Landau theory, phase transitions are characterized by two temperatures $T_c$ and $\theta_s$. $T_c$ is a measure for the collective forces which have to be compensated by thermal forces in order to achieve the low symmetry form at $T < T_c$. $\theta_s$ is a measure for the anharmonnicity of the system which is related to the saturation of the order parameter at low temperature. At $T < T_s = 1/2\ \theta_s$, the order parameter nearly independent of temperature. At high temperatures, $T > \theta_s$, the expression in Eq. (5) proves to be independent of $\theta_s$, i.e. the classical Landau-type free energy. Least-squares curve-fitting was performed to obtain $\beta$, $T_c$ and $\theta_s$. An excellent agreement between experimental observation and theoretical prediction has been found, as shown in Fig. 6, where the lines represent the prediction from generalized Landau theory and the open symbols indicate experimental observations. The fitting results in averaged $\beta = 0.26 \pm 0.02$ and $T_c = 226 \pm 3$ K, suggesting that the transition is close to a tricritical type. The transition temperature obtained from infrared data is well consistent with the reported value (228 K). The data analysis shows that different types of infrared bands appear to give different values of $\theta_s$. The Si–O bending near 538 $cm^{-1}$ exhibits a value of $\theta_s$ of $91 \pm 5$ K. The vibration near 688 $cm^{-1}$ associated with the $Si_2O_6$ chains shows a smaller value of $\theta_s$ ($56 \pm 6$ K). Our observation of the different values of $\theta_s$, which do not appear in quartz or other materials, could be experimental evidence, for the first time, supporting the complex mode coupling proposed by Pérez-Mato and Salje (2001), although it is difficult to estimate the potential experimental uncertainties related to the determination of $\theta_s$ at this stage.

In summary, the experimental results from this infrared study show that $LiFeSi_2O_6$ undergoes a structural phase transition (from $C2/c$ to $P2_1/c$) with decreasing temperatures. The structural phase transition is characterized by the appearance of extra bands at 154, 213, 232, 280, 302, 453, 508, 537, 688, 767, 985, 1068 and 1138 $cm^{-1}$ (the frequency values for 220 K). The transition is associated with dramatic changes in spectral patterns due to new Li coordination. The appearance of extra bands in the region of the Si–O–Si vibrations in $Si_2O_6$ chains are observed and this suggests the formation of two independent silicate chains, supporting previous observations by X-ray diffractions. Low-frequency infrared bands show strong frequency shift with decreasing temperature. However, the frequencies of the Si–O-stretching bands of $SiO_4$ tetrahedra show very weak temperature dependence or almost temperature independence upon cooling. This indicates that the $SiO_4$ tetrahedra are basically very rigid and the bond distance between Si and O shows no significant change. Anomalous spectral changes in $LiFeSi_2O_6$ are recorded in the frequency region of 300 and 330 $cm^{-1}$. In comparison with the data of $NaFeSi_2O_6$, the changes are explained as the consequence of mode crossing in the frequency region. A generalized Landau theory is used to study the behaviour of the order parameter, $Q$. The analysis of the order parameter lead to $\beta = 0.26 \pm 0.02$, and $T_c = 226 \pm 3$ K, indicating that the transition is close to tricritical.

## References


Baum E, Treutmann W, Behruzi M, Lottermoser W, Amthauer G (1988) Structural and magnetic properties of the clinopyroxenes $NaFeSi_2O_6$ and $LiFeSi_2O_6$. Z Kristallogr 183:273–284

Behruzi M, Hahn T, Prewitt CT, Baldwin K (1984) Low- and high-temperature crystal structures of $LiFeGe_2O_6$, $LiFeSi_2O_6$ and $LiCrSi_2O_6$. Acta Crystallogr (A)40 Suppl C-247

Cho SM, Jang HM (2000) Softening and mode crossing of the lowest-frequency $A_1$ (transverse-optical) phonon in single-crystal $PbTiO_3$. Appl Phys Lett 76:3014–3016

Choudhury N, Ghose S, Chowdhury CP, Loong CK, Chaplot SL (1998) Lattice dynamics, Raman spectroscopy, and inelastic neutron scattering of orthoenstatite $Mg_2Si_2O_6$. Phys Rev (B) 58:756–765

Clark, JR, Appleman, DE, Papike, JJ (1969) Crystal-chemical characterization of clinopyroxenes based on eight new structure refinements. Mineral Soc Am Spec Pap 2:31–50

Farmer VC (1974) Orthosilicate, pyrosilicates, and other finite-chain silicates. In Farmer VC (ed) The infrared spectra of minerals. Mineralogical Society, London, pp 285–303

Huang E, Chen CH, Huang T, Lin EH, Xu JA (2000) Raman spectroscopic characteristics of Mg–Fe–Ca pyroxenes. Am Mineral 85:473–497

Lazarev AN (1972) Vibrational spectra and structure of silicates. Consultants Bureau, New York, pp 101–102

Landau LD, Lifshitz EM (1980) Statistical physics. Pergamon, Oxford

Lottermoser W, Redhammer G, Forcher K, Amthauer G, Paulus W, Andre G, Treutmann W (1998) Single-crystal Mössbauer and neutron powder diffraction measurements on the synthetic clinopyroxene Li-acmite $LiFeSi_2O_6$. Z Kristallogr 213:101–107

McMillan P (1984) Structural studies of silicates glasses and melts – applications and limitations of Raman spectroscopy. Am Mineral 69:622–644

Mysen BO (1990) Relationship between silicate melt structure and petrologic processes. Earth Sci Rev 27:281–365

Pérez-Mato JM, Salje EKH (2001) Order-parameter saturation at low temperatures: displacive phase transitions with coupled Einstein oscillators. Philos Mag Lett 81:885—891

Redhammer GJ, Roth G (2002) Structural variations in the aegirine solid-solution series (Na,Li)$FeSi_2O_6$ at 298–80 K. Z Kristallogr (in press)

Redhammer GJ, Amthauer G, Lottermoser W, Treutmann W (2000) Synthesis and structural properties of clinopyroxenes of the hedenbergite $CaFe^{2+}Si_2O_6$-aegirine $NaFe^{3+}Si_2O_6$ solid-solution series. Eur J Mineral 12:105–120

Redhammer GJ, Roth G, Paulus W, André G, Lottermose W, Amthauer G, Treutmann W, Koppelhuber-Bitschnau B (2001) The crystal and magnetic structure of Li-aegirine $LiFe^{3+}Si_2O_6$: a temperature-dependent study. Phys Chem Miner 28:337–346

Ross NL, Reynard B (1999) The effect of ion on the $P2_1/c$ to $C2/c$ transition in (Mg,Fe)$SiO_3$ clinopyroxenes. Eur J Mineral 11:585–589

Rutstein MS, White WB (1971) Vibrational spectra of high-calcium pyroxenes and pyroxenoids. Am Mineral 56:877–887

Saksena BD (1961) Infrared absorption studies of some silicate structures. Trans Faraday Soc 57:242–258

Saksena BD, Agarwal KC, Jauhri GS (1963) The rign band of cyslo-silicates. Trans Faraday Soc 59:276–283

Salje EKH, Bismayer U (1997) Hard mode spectroscopy: the concept and applications. Phase Transitions 63:1–75

Salje E, Wruck B, Marais S (1991a) Order parameter staturation numerical results for displacive and O/D systems. Ferroelectrics 38:77–97

Salje E, Wruck B, Thomas H (1991b) Order-parameter saturation and a low-temperature extension of Landua theory. Z Phys B Conden Matter 82:399–404

Teeters D, Frech R (1982) Temperature dependence of the Raman-active lithium modes in $LiKSO_4$ and $LiNaSO_4$. Phys Rev B 26, 4132–4139

Wang A, Jolliff BL, Haskin LA, Kuebler KE, Viskupic KM (2001) Characterization and comparison of structural and compositional features of planetary quadrilateral pyroxenes by Raman spectroscopy. Am Mineral 86:790–806

Zhang M, Wruck B, Graeme-Barbar A, Salje EKH, Carpenter MA (1996) Phonon spectroscopy on alkali-feldspars: phase transitions and solid solutions. Am Mineral 81:92–104

Zhang M, Salje EKH, Putnis A (1998) Phase transitions in $LiKSO_4$ between 1.5 K and 850 K: an infrared spectroscopic study. J Phys Condens Matter 10:11811–11827

Zhigadlo ND, Zhang M, Salje EKH (2001) An infrared spectroscopic study of $Li_2B_4O_7$. J Phys Condens Matter 13:6551–6561